

Double core-hole spectroscopy of transient plasmas produced in the interaction of ultraintense x-ray pulses with neon

Cheng Gao¹, Jiaolong Zeng¹, and Jianmin Yuan^{1,2}

¹Department of Physics, College of Science, National University of Defense Technology, Changsha Hunan 410073, P. R. China

²IFSA Collaborative Innovation Center, Shanghai Jiao Tong University, Shanghai 200240, P. R. China

E-mail: jlzeng@nudt.edu.cn, jmyuan@nudt.edu.cn

Abstract.

Double core-hole (DCH) spectroscopy is investigated systematically for neon atomic system in the interaction with ultraintense x-ray pulses with photon energy from 937 eV to 2000 eV. A time-dependent rate equation, implemented in the detailed level accounting approximation, is utilized to study the dynamical evolution of the level population and emission properties of the highly transient plasmas. For x-ray pulses with photon energy in the range of 937-1030 eV, where $1s \rightarrow 2p$ resonance absorption from single core-hole (SCH) states of neon charge states exist, inner-shell resonant absorption (IRA) effects play important roles in the time evolution of population and DCH spectroscopy. Such IRA physical effects are illustrated in detail by investigating the interaction of x-ray pulses at a photon energy of 944 eV, which corresponds to the $1s \rightarrow 2p$ resonant absorption from the SCH states ($1s2s^22p^4$, $1s2s2p^5$ and $1s2p^6$) of Ne^{3+} . After averaging over the space and time distribution of the x-ray pulses, DCH spectroscopy at photon energies of 937, 944, 955, 968, 980, and 990 eV (corresponding to the $1s \rightarrow 2p$ resonance energies of Ne^{2+} - Ne^{7+} , respectively) are studied in detail. The complex mechanisms of producing the DCH states are discussed, taking the DCH spectroscopy at 937 and 980 eV as examples. For photon energy larger than 1362 eV, there are no resonance absorption in the interaction, resulting in a similar physical picture of DCH spectroscopy. The dominant DCH states are due to higher ionization stages of Ne^{7+} - Ne^{9+} , while the DCH spectroscopy from lower charge states Ne^{2+} - Ne^{6+} are much weaker. With the increase of x-ray photon energy, the contributions from the lower charge states become larger.

PACS numbers: 32.30.-r, 32.80.Aa

1. Introduction

Production of double core-hole (DCH) states represents a quite recent experimental achievement by using synchrotron radiation and x-ray free-electron lasers (XFELs) [1]. Two main experimental methods have been used to induce such highly transient quantum states with a lifetime of ~ 1 femtosecond (fs). One is by using synchrotron radiation and then single photon inner-shell photoionization occurs followed by the simultaneous ejection of two core electrons. The other is by using XFELs and multiple-photon absorption, resulting in the production of DCH states via sequential absorption of two x-ray photons on a time scale of a few fs. The probability of the former method is in general much smaller than the latter by using ultraintense x-ray pulses. As is well known, the intensity of x-ray radiation produced by synchrotron radiation is smaller than that of XFELs by more than six orders of magnitudes and hence creation of DCH states by sequential photoionization was not possible. However, such a case is changed by the ultraintense XFEL pulses such as the Linac Coherent Light Source (LCLS) [2] and the Spring-8 Angstrom Compact free electron LAsER (SACLA) [3]. With the new generation light source, hollow atoms and molecules are readily produced [4, 5, 6, 7, 8, 9, 10, 11].

DCH spectroscopy carries on rich information on the transient plasmas created in the interaction of x-ray pulses with matters (atoms, molecules, clusters, and solid-state matter) and therefore it has practical applications in many aspects. Compared with conventional inner-shell photoelectron spectroscopy, it has unique features in the investigations of such highly transient plasmas [12]. Auger electrons emitted from DCH states are a distinctive signature of hollow atom formation and hence electron spectra can act as the evidence of hollow atoms. Recently, investigations carried out by Berrah *et al.* [6], Salen *et al.* [9] and Takahashi and Ueda [13] experimentally verified that DCH spectroscopy provides a powerful means for chemical analysis. It has shown that it has greater potential to probe the local chemical environment than by detecting single core-hole (SCH) spectroscopy. Secondly, combining with accurate theoretical simulations [14], DCH spectroscopy provides a useful tool for estimating or even diagnosing the intensity and duration of x-ray pulses [15]. In dense plasmas, it reflects the screening effects on atoms embedded in the plasmas produced by x-ray laser pulses [16, 17, 18, 19] and thus it can be utilized to deduce the environmental effects.

Neon is a prototype object to investigate the interaction with high-intensity and short duration x-ray pulses [5, 20, 21, 22, 23, 24]. However, detailed and systematic investigations of the DCH spectroscopy on this object are lacking very much. Young *et al.* [5] experimentally observed the existence of DCH states of neon at a photon energy of 1050 eV by measuring the electron spectra at the direction of incident x-ray polarization. To the best of our knowledge, no measurements are available for the emission spectra produced by the DCH states of neon. Our understanding on the DCH states and spectroscopy for neon interacting with XFELs is rather limited and incomplete. It is worthwhile to systematically study it over a wide range of photon energy.

In this work, we systematically investigate the emission properties of DCH states of transient neon plasmas created in the interaction of XFELs with photon energy ranging from 937 eV to 2000 eV. A time-dependent rate equation (TDRE) approach [23, 25, 26] based on the collisional-radiative model is employed to study the evolution dynamics of charge state distribution (CSD) and emission properties. A detailed level accounting (DLA) model is utilized to describe the quantum states of the neon system. The DLA model has been proved to be one of the most accurate method in the computation of the radiative opacity of hot dense plasmas in local thermodynamic equilibrium [27, 28, 29, 30]. It is also one of the most accurate method to describe the XFELs interaction with atoms. Based on the TDRE and DLA approaches, we systematically investigated the DCH spectroscopy for the XFELs interaction with neon at different photon energy over a wide range. For the x-ray pulses, we assume Gaussian profiles for the spatial, time and frequency distribution.

2. Theoretical methods

In the treatment of the interaction of XFELs with atoms, we utilized a DLA formalism, where the quantum states of our concerned physical system are accurate to fine-structure level. The population n_i of the fine-structure level i is obtained by solving the rate equation

$$\frac{dn_i}{dt} = \sum_{j \neq i}^{N_L} n_j R_{ji} - n_i \sum_{j \neq i}^{N_L} R_{ij}, \quad (1)$$

where R_{ij} and R_{ji} represent the rates which depopulate and populate between the levels i and j and N_L is the total number of levels included in the calculation. The levels of all ionization stages from the neutral to fully stripped neon ions are included up to principal quantum number $n=4$ with SCH and DCH states being taken into account. The rates connecting different levels include all main microscopic atomic processes due to photons and electrons, namely photo-excitation, photoionization, electron impact excitation, electron impact ionization, Auger decay and their inverse processes [31, 32].

The rate due to photons (radiation field) is determined by the cross sections of corresponding microscopic process [33, 34]

$$R_{ij}(r, t) = \int \frac{I(r, t, h\nu)}{h\nu} \sigma_{ij}(h\nu) d(h\nu), \quad (2)$$

where $I(r, t, h\nu)$ is the XFEL intensity at space position r from the center of the laser spot, time t and the photon frequency ν , and $\sigma_{ij}(h\nu)$ is the photoexcitation or photoionization cross section at photon energy $h\nu$. The intensity of XFELs is assumed to have a Gaussian profile on the space, time and photon frequency

$$I(r, t, h\nu) = I_0 e^{-\ln 2 (\frac{r}{\Delta})^2} e^{-\ln 2 (\frac{t}{\tau})^2} \sqrt{\frac{\ln 2}{\pi \Gamma^2}} e^{-\ln 2 (\frac{h\nu - h\nu_0}{\Gamma})^2}, \quad (3)$$

where I_0 is the peak intensity and $h\nu_0$ is the photon energy of the x-ray pulse. Δ , τ and Γ are the half width at half maximum (HWHM) of Gaussian profile of the x-ray

pulse on the distribution of space, time and photon energy, respectively. Note that the dependence of intensity on photon energy (frequency) has been multiplied by a constant quantity to satisfy the normalization (to 1). The energy of x-ray pulses can be obtained by integrating the intensity over the space, time and photon energy over all possible variable regions. Such a quantitative connection of pulse energy and intensity can help us to better understand the physics of the interaction. The initial density of neon is taken to be $1.0 \times 10^{17} \text{ cm}^{-3}$ in this work and thus the rates due to electrons are small compared with those of photons and Auger decay rates [23]. The details on the atomic model and atomic data can be found elsewhere [31]. Briefly, we include the quantum states of single and double excitation states including core-hole ($1s$) states up to principal quantum number $n=4$ for all ionization stages from the neutral atom to bare ion in the rate equation. The required atomic data including the spontaneous radiative decay rate, photoionization and photo-excitation cross section, and Auger decay rate connecting all these levels are obtained by solving a relativistic Dirac equation [35]. The direct double Auger decay rates are obtained by using simplified formulas according to the knock-out (KO) and shake-off (SO) mechanisms as we demonstrated [36, 37, 38, 39].

After solving the rate equation, we obtain the level populations which can be used to calculate the emission properties of plasmas. The emissivity $j(h\nu)$ at photon energy $h\nu$ due to DCH states reads as

$$j(h\nu) = \sum_{j>i} n_j h\nu A_{ji} S(h\nu), \quad (4)$$

where n_j is the population of the upper level of the transition $j \rightarrow i$, A_{ji} and $S(h\nu)$ are the radiative transition probability and line profile of the transition $j \rightarrow i$, respectively. $S(h\nu)$ is taken to be a Lorentian profile to account for both the natural lifetime broadening and autoionization width. If we only consider the DCH spectroscopy, we limit the summation on the upper levels which are DCH states.

3. Results and discussions

To produce DCH states, the lowest photon energy should be high enough to ionize or excite two $1s$ electrons of the neutral neon. As we know, the ionization potential (IP) will increase for the $1s$ electron from the SCH state compared to IP from levels of ground configuration, hence the way with lowest energy should be photoionizing the first $1s$ electron and then photo-exciting another $1s$ electron to $2p$. To have a quantitative understanding, we give the single and double ionization potential (SIP and DIP) of $1s$ electrons from the atomic to hydrogen-like neon in table 1. Note that hydrogen-like neon has only one electron and thus there is no DIP for it. The experimental values are given wherever available for atomic Ne [40], Ne^{4+} - Ne^{6+} [41] and Ne^{8+} [42]. For those ions where no experimental results are available, our theoretical results are given. From the inspection of table 1, we see that the $1s$ SIP of atomic neon is 870.3 eV [40] and the lowest DIP is 986.0 eV for Ne^{2+} (production of $1s^0 2s^2 2p^6$). It seems that the lowest photon energy which can produce DCH states is 986.0 eV. This conclusion is correct

if one only considers the direct photoionization channels. However, if we include the resonance absorption from the SCH states, the above physical picture will be modified. To have an overall view of the resonance absorption of $1s \rightarrow 2p$, we show the absorption cross sections from all possible energy levels belonging to the configurations of $1s2s^m2p^n$ ($m+n=8-0$, corresponds to Ne^{1+} - Ne^{9+} , respectively) in Fig. 1. The result is obtained by summing the photoexcitation cross section of resonance absorption $1s \rightarrow 2p$ from all levels of $1s2s^m2p^n$ of all possible charge states

$$\sigma(h\nu) = \sum_{j>i} \frac{\pi h e^2}{m_e c} f_{ij} S(h\nu), \quad (5)$$

where h is the Planck constant, m_e is the electron mass, $S(h\nu)$ is the line profile. A Lorentian profile is assumed with natural lifetime broadening and autoionization width being taken into account.

From the inspection of Fig. 1, we can determine that the lowest photon energy which can produce DCH states is ~ 937.0 eV, which is the resonance energy of $1s2s^22p^5 \rightarrow 1s^02s^22p^6$ for Ne^{2+} . Photons with this energy can first effectively ionize atomic neon and Ne^{1+} and then produce DCH state $1s^02s^22p^6$ (Ne^{2+}) by resonance photo-excitation process. Actually, there are many resonance absorptions from different ionization stages in the photon energy range 935.0 eV-1030.0 eV. First, we point out that the resonance absorption for x-ray photons with an energy in this range plays an important role in the evolution dynamics of population and DCH spectroscopy just as we demonstrated previously [33]. We take the x-ray pulse with photon energy of 944 eV as an example to illustrate the effects of resonance absorption on the evolution dynamics of the fractions of different charge states and of the population fractions of the SCH and DCH states, which are shown in Figs. 2 and 3 for an x-ray pulse with peak intensity $I_0=2 \times 10^{17}$ W/cm² and duration $\tau=50$ fs at a photon energy of 944 eV. To obtain the result, we set a bandwidth Γ to be 3 eV.

X-ray pulse with an energy of 944 eV can photoionize one $1s$ electron of Ne - Ne^{2+} to form SCH states of Ne^{1+} - Ne^{3+} , yet it cannot ionize $1s$ electron of Ne^{3+} as the photon energy is smaller than the SIP of Ne^{3+} (see table 1). However, there are inner-shell resonant absorption (IRA) channels for Ne^{3+} . After the photoionization of $1s$ electron of Ne^{2+} , SCH states belonging to the configuration $1s2s^22p^4$ of Ne^{3+} is produced. Then the DCH states $1s^02s^22p^5$ of Ne^{3+} are effectively produced by the $1s \rightarrow 2p$ IRA process. The reason for the effectiveness of such processes lies in the large absorption cross section near the resonances. The physical effects of IRA on the evolution dynamics of populations can be seen in Fig. 2. The results have been averaged over the spatial distribution of the light spot. The detailed method of averaging over the space can be found in our work [43]. To save space, the dependence of fraction evolution on the space is not explicitly given here. From the inspection of Fig. 2, one can see that the IRA effects do not affect the fraction evolution of Ne^{1+} and Ne^{2+} , yet they have strong effects on higher ionization stages, in particular for Ne^{4+} - Ne^{5+} . With the inclusion of the resonance channels in the rate equation, the fraction of Ne^{4+} is dramatically decreased, while that of Ne^{5+} is greatly enhanced. Such a decrease for Ne^{4+} and increase for Ne^{5+}

begin at -75 fs and the relative difference becomes larger with the increase of time. The zero point of time is chosen at the moment of peak intensity of x-ray laser. At the time of 0 and 50 fs, the fraction of Ne^{4+} is decreased by 47% and 55% and that of Ne^{5+} is increased by 135% and 93%, respectively. The fractions of Ne^{6+} - Ne^{7+} are also evidently enhanced with higher relative difference. Such a conclusion is easy to understand. The DCH states of Ne^{3+} decay dominantly to the SCH states of Ne^{4+} by Auger processes, which further decay to Ne^{5+} .

The effects of IRA processes can further be seen from the time evolution of the fractions of DCH and SCH states produced in the interaction, which are shown in Fig. 3. Without inclusion of IRA channels, the populations of DCH states of neon charge states are very small ($\sim 10^{-9}$) and thus they are not shown in panel (a). Hence we can safely say that the DCH states at a photon energy of 944 eV are dominantly due to the resonance absorption channels from the SCH states of Ne^{3+} . In panel (b), the populations of SCH states of Ne^{5+} - Ne^{7+} without IRA effects are not shown for the same reason. For SCH states, there is little difference between the populations of Ne^{1+} - Ne^{3+} with and without the consideration of IRA processes. However, there are large discrepancies for the populations of higher charge states. For Ne^{4+} , the peak value of the population (at -30fs) with IRA effects is about 50 times larger than the corresponding value of without IRA effects. The SCH populations of Ne^{5+} - Ne^{7+} with IRA effects (relative difference) are even much larger than the corresponding values without IRA effects. These discrepancies originate from the formation of DCH states of Ne^{3+} and the followed Auger decay to SCH states of Ne^{4+} . The large discrepancies of the populations of DCH and SCH with and without IRA effects lead to the discrepancies on the spectra accordingly.

From the above discussion, we know that the IRA processes have profound effects on the time evolution of populations, especially for the DCH states. Without the opening of the resonance absorption channels, the populations of the DCH states are negligibly small. The populations will be enhanced by more than six orders of magnitudes if we take the IRA processes into account. To have a more complete picture of the CSD, we show it in Fig. 4 after spatially and temporally averaging. The effects of IRA processes can readily be seen from this figure. Overall, including IRA effects, the fraction of Ne^{4+} is decreased by 49%, while the fractions of Ne^{5+} - Ne^{7+} are increased by 114%, 148%, 180%, respectively.

The prominent effects of IRA processes on the populations tell us that we must include them in the rate equation to obtain accurate results. In the following, these effects have been considered and therefore we do not state it again. As an example, Fig. 5 shows the time evolution of emissivity of neon interacting with an x-ray pulse (photon energy 944 eV) with a peak intensity of $I_0=2\times 10^{17}$ W/cm² and duration $\tau=50$ fs at time -50, 0, and 50 fs. In general, the emissivity decreases rapidly from $t=-50$ fs to $t=0$ fs and then decreases smoothly from $t=0$ to $t=50$ fs. Two distinctive features appear in the photon energy ranges of 830-930 eV and 930-1030 eV with the former one produced by the SCH states and the latter one by DCH states. The structures at lower

energy range are dominantly contributed by Ne^{1+} - Ne^{4+} , while at higher energy range only Ne^{3+} contributes the largest emissivity.

After the irradiation of x-ray laser pulses, the emissivity of the highly transient plasma is shown in Fig. 6 by averaging over the whole space and time region. The dramatic effects due to IRA processes can readily be seen from the comparison of the results with and without the IRA channels being included. Without the opening of IRA channels, only the SCH states of Ne^{1+} - Ne^{3+} contribute to the emission spectra and the SCH states of Ne^{4+} - Ne^{5+} have negligibly small contribution. More clearly, the emission features of DCH states above photon energy of 930 eV are nearly completely invisible. The high efficiency of resonance absorption of $1s \rightarrow 2p$ for the production of DCH states can be seen from this figure. We can also observe that the emission spectra of SCH and DCH states have different characteristics. The quasi-continuous band of the DCH states is broader than that of SCH ones for the same charge state.

In the above, we investigated the dynamical evolution of the CSD and emissivity of transient plasmas produced in the interaction of neon with x-ray laser pulses at a photon energy of 944 eV. The overall emission features due to SCH and DCH states are discussed. In the following, we focus our attention to the DCH spectroscopy. From Fig. 1, we know that the lowest photon energy to produce DCH states is 937 eV, at which the DCH states are created by the $1s \rightarrow 2p$ resonance absorption, just as we have just discussed in the above for $h\nu_0=944$ eV. We study the emissivity at two different photon energy ranges of 930-1030 eV and above 1362 eV. In the former region, the dominant mechanism of producing DCH states is first photoionizing one $1s$ electron of neon ions and then sequentially photoexciting another $1s$ electron by $1s \rightarrow 2p$ resonance absorption. In the latter region, the radiation field sequentially photoionizes two $1s$ electrons one by one and then the DCH states are produced.

We first investigate the DCH spectroscopy in the former photon energy region where the resonance absorption exists. Figure 7 shows the emissivity at six typical photon energies of 937, 944, 955, 968, 980, and 990 eV, which are the central $1s \rightarrow 2p$ resonance energy from the SCH states of Ne^{2+} - Ne^{7+} , respectively. The emission spectra at 944 eV have just been discussed detailedly in the above. The x-ray pulses are assumed to have a peak intensity of 2×10^{17} W/cm² and duration of 50 fs in all cases. From the inspection of panels (a)-(e) of Fig. 7, we can see evident DCH emissions from Ne^{2+} - Ne^{7+} ions. In general, the emissivity increases with the increase of the photon energy except for that at 968 eV. The common feature for all six cases is that prominent emission occurs at only around the resonance energies. This is in agreement with the production mechanism discussed in the above. From the IP of the DCH states for Ne - Ne^{9+} ions shown in table 1, we know that sequential photoionization of two $1s$ electrons can only be accessible for Ne^{2+} at photon energy higher than 986 eV. This is because the photoionization channels of $1s$ electrons from SCH states $1s2s^22p^6$ of Ne^{1+} are opened at 990 eV and therefore the DCH state $1s^02s^22p^6$ of Ne^{2+} is effectively produced. Such a fact is reflected in the emission spectra at 990 eV (Fig. 7(f)). Besides the dominant emission features around the photon energy of 990 eV, a clean emission structure located

at 937 eV appears in Fig. 7(f).

For all other five cases with photon energy lower than 986 eV shown in Fig. 7(a)-(e), the structure at 937 eV does not appear. However, new emission characteristics are observed besides the above common feature. At the photon energy of 944 and 955 eV, the emission spectra are relatively pure and are dominantly due to the $2p \rightarrow 1s$ transitions from DCH states of Ne^{3+} and Ne^{4+} . Yet for other cases, there are additional structures caused by nearby ions. At 937 eV (resonance energy of Ne^{2+}), the emission from Ne^{3+} is even stronger than Ne^{2+} . At 968, 980, and 990 eV, which corresponds to the central resonance energies of Ne^{5+} , Ne^{6+} , and Ne^{7+} , respectively, emissions from nearby ions are evident in the emissivity.

How are the emissions from the nearby ions happened? In what follows, we analyze the origin of these emission structures produced by nearby ions by considering the results shown in Fig. 7(a) and 7(e) at 937 and 980 eV as examples. First, we pay attention to the emissivity at 937 eV. The emission line located at 937 eV originates from $2p \rightarrow 1s$ transitions from level $1s^0 2s^2 2p^6$ to $1s 2s^2 2p^5$ of Ne^{2+} . Around and lower than 937 eV, there are some structures except for that emitted by Ne^{2+} . These emissions originate from the SCH states produced by the resonance absorption $1s \rightarrow 3p$ from levels belonging to configuration $1s^2 2s^2 2p^3$ of Ne^{3+} , as shown in table 2 (Nos. 1-9). Once SCH states $1s 2s^2 2p^3 3p$ are produced, they radiatively decay to the levels of the ground configuration $1s^2 2s^2 2p^3$, resulting in the emissions at photon energy range of lower than 937 eV. The strongest emission centered at 944 eV originates from the DCH states of Ne^{3+} . It seems that DCH states of Ne^{3+} cannot be produced at 937 eV, which is the resonance energy of Ne^{2+} . Intuitive feeling tells us that higher photon energy is needed to create DCH states of Ne^{3+} . Yet there are channels for such a production and the mechanism can be explained as follows. After the creation of DCH state $1s^0 2s^2 2p^6$ for Ne^{2+} , it decays dominantly by Auger processes to SCH levels belonging to the configurations of $1s 2s^2 2p^4$, $1s 2s 2p^5$, and $1s 2p^6$ of Ne^{3+} . From levels of $1s 2s 2p^5$, there are $1s \rightarrow 2p$ resonances to produce DCH state $1s^0 2s 2p^6$ of Ne^{3+} (see Nos. 10-11 in table 2) with resonance energy of ~ 937.5 eV, which is very close to 937 eV. In such a way, DCH state $1s^0 2s 2p^6$ of Ne^{3+} are produced. Then it decays to the lower levels of $1s 2s 2p^5$ radiatively to emit at ~ 944 eV (transitions Nos. 12-13 in table 2). Due to the fine structure splitting of $1s 2s 2p^5$, the resonance energy is located at ~ 937 eV for those levels with higher energies, while it is located at ~ 944 eV for those levels with lower energies. As the oscillator strengths of transitions (Nos. 12-13 in table 2) are very large, resulting in the strong emission at ~ 944 eV.

Secondly, we turn to the emissivity at photon energy of 980 eV ($1s \rightarrow 2p$ resonance energy of Ne^{6+}), which is shown in Fig. 7(e). DCH spectroscopy of Ne^{5+} and Ne^{6+} is evident in the figure, yet the production mechanism of DCH states is different from that at 937 eV. From the inspection of table 1, we know that photons with energy of 980 eV can ionize one $1s$ electron of Ne^{3+} , yet they do not have enough energy to ionize one $1s$ electron of Ne^{4+} and higher charge states. Hence it is impossible to produce DCH states of Ne^{6+} by first creation of $1s 2s^m 2p^n$ ($m+n=3$) of Ne^{6+} from single $1s$ photoionization

and then produce DCH states by $1s \rightarrow 2p$ resonance absorption. Because of this, there is no emission from Ne^{6+} at 980 eV. Then how are the DCH states of Ne^{5+} and Ne^{6+} produced? What kind of K-shell hollow states are they? As we just discussed, photons with energy of 980 eV can ionize one $1s$ electron up to Ne^{3+} forming the SCH states (dominated by $1s2s^22p^3$, $1s2s2p^4$, and $1s2p^5$) of Ne^{4+} , which mainly decay to levels of $1s^22s^22p$, $1s^22s2p^2$ and $1s^22p^3$ of Ne^{5+} . From these levels, there are $1s \rightarrow 3p$ resonance absorption channels of Ne^{5+} to form SCH states of $1s2s^m2p^n3p$ ($m+n=3$), which can further be photoexcited by $1s \rightarrow 2p$ resonance to form the DCH states $1s^02s^m2p^n3p$ ($m+n=4$) of Ne^{5+} . To have a direct understanding of these resonance channels, the absorption cross sections of the above two types of resonant transitions are shown in Fig. 8(a). Many strong resonant absorptions are centered at photon energy of 980 eV to form quasi-continuum bands. The channels can effectively produce the DCH states of Ne^{5+} and result in the emission around 980 eV. Once DCH states $1s^02s^m2p^n3p$ ($m+n=4$) of Ne^{5+} are produced, they decay by Auger processes dominantly to levels of $1s2s^m2p^n3p$ ($m+n=2$) of Ne^{6+} . From these levels, there are also many $1s \rightarrow 2p$ resonance absorption with the strongest peak being at 990 eV. Although the resonances at 980 eV are weak compared with the stronger ones, the absorption cross section (quasi-continuum band around 980 eV) is far larger than the direct photoionization cross section of $2s$, $2p$, and $3p$ electrons and therefore create effective channels to form DCH states of $1s^02s^m2p^n3p$ ($m+n=3$) of Ne^{6+} . The above conclusion can be seen from Fig. 8(b), which shows the absorption cross sections of $1s \rightarrow 2p$ resonances from $1s2s^m2p^n3p$ of Ne^{6+} . Once DCH states $1s^02s^m2p^n3p$ of Ne^{6+} are produced, they decay by radiative processes to the SCH states of $1s2s^m2p^n3p$ by $2p \rightarrow 1s$ centered at 990 eV. The emissions centered at ~ 1004 eV are mainly due to $3p \rightarrow 1s$ transitions from SCH states of $1s2s^m2p^n3p$ of Ne^{6+} .

From the above discussion, we know that the production of DCH states of Ne^{5+} and Ne^{6+} are rather complicated at photon energy 980 eV. In particular, the DCH states of Ne^{6+} originate from the weak resonances and the DCH spectroscopy shows special features. The emissivity is very sensitive to the laser intensity, as demonstrated in Fig. 9, which shows the DCH spectroscopy at laser intensities of 1×10^{16} , 3×10^{16} , 5×10^{16} , and 1×10^{17} W/cm². At the intensity of 1×10^{16} W/cm², the dominant DCH emissions originate from Ne^{5+} ($2p \rightarrow 1s$) centered at 980 eV, while the DCH spectroscopy from Ne^{6+} centered at 990 eV is nearly invisible. The emission structures around 1004 eV originate from the SCH state transitions ($3p \rightarrow 1s$) to levels of $1s^22s^m2p^n$ ($m+n=2$) for Ne^{6+} . With the increase of laser intensity, the DCH emissivity from Ne^{6+} becomes larger and larger and the peak value exceeds that of Ne^{5+} at the intensity of $\sim 6 \times 10^{16}$ W/cm².

In the above, we investigated in detail the DCH spectroscopy at photon energy region where there exist strong resonance absorptions of $1s \rightarrow 2p$ from the SCH states of different ionization stages of neon. In what follows, we turn to the DCH spectroscopy at photon energy range of larger than 1362 eV, where no resonance absorption exists. Figure 10 shows the DCH spectroscopy at photon energies of 1400, 1600, 1800, and 2000 eV. The laser intensity and duration are taken to be the same values as in the

above ($I_0=2\times 10^{17}$ W/cm² and $\tau=50$ fs). For x-rays in this photon energy range, the creation mechanism of DCH states is simple. By sequentially absorbing two photons, the DCH states of different ionization stages can be produced. With the increase of photon energy, the emissivity decreases from Fig. 10(a)-10(d). At lower photon energy, the photoionization cross section is larger and therefore it is more efficient to photoionize neon ions than at higher energy. The fact of larger cross section at lower photon energy also explains the reason that the emissivity from the DCH states of higher ionization stages are stronger than at higher energy. In all cases, the emissions from DCH states of Ne²⁺-Ne⁶⁺ are weak, while they increase with the increase of x-ray photon energy.

In this work, XFELs are assumed to have short temporal coherence and the coherence effects are neglected. At present day, XFELs work at a mode of self-amplified spontaneous emission and the longitudinal coherence is not good [4]. Recently, Ackermann *et al.* [44] reported the first seeded XFELs, which generated highly coherent source of radiation with a very long temporal coherence. For such coherent XFELs, one has to consider the quantum coherence effects in the dynamical excitation, ionization, and decay processes of the produced transient plasmas. Li *et al.* [45] developed a large scale quantum master equation approach to deal with such real dynamical evolution driven by the coherent XFELs. The physical effects due to the longitudinal coherence of XFELs are clearly demonstrated in this reference.

4. Conclusion

Neon interacting with ultraintense x-ray pulses is investigated by using a time-dependent rate equation implemented in the detailed level accounting approximation. The double core-hole (DCH) spectroscopy is investigated systematically for x-ray pulses with different photon energy ranging from 937 eV to 2000 eV, which covers two distinct regions with different features. The region with lower energy from 937 to 1030 eV, there exist many strong $1s \rightarrow 2p$ resonances from the SCH states of Ne²⁺-Ne⁸⁺. Yet in another region with photon energy higher than 1362 eV there are no resonance absorption for any ionization stage of neon. In the resonance region, inner-shell resonant absorption (IRA) effects play important roles on dynamical evolution of the level populations and emission properties of the highly transient plasmas produced in the interaction, in particular for the DCH states. The IRA effects are exemplified by studying the interaction of x-ray pulses at a photon energy of 944 eV, which corresponds to the $1s \rightarrow 2p$ resonant absorption from the SCH states ($1s2s^22p^4$, $1s2s2p^5$, and $1s2p^6$) of Ne³⁺. The population of DCH states is dramatically enhanced (more than six orders of magnitudes) compared with that without the consideration of IRA. The DCH spectroscopy at six typical photon energies of 937, 944, 955, 968, 980, and 990 eV is investigated in detail. These photon energies correspond to the $1s \rightarrow 2p$ resonance energies of Ne²⁺-Ne⁷⁺. At 944 and 980 eV, the mechanisms of producing the DCH states are detailedly studied. For x-ray pulses with photon energy larger than 1362 eV (where no resonances absorption exist), the DCH spectroscopy shows completely different features compared with that at 937-1030

eV. DCH states from all possible ionization stages of Ne^{2+} - Ne^{8+} can be produced by multiple photon ionization. Yet the dominant DCH states are due to higher ionization stages of Ne^{7+} - Ne^{8+} . With the increase of photon energy, the contributions from the lower charge states Ne^{2+} - Ne^{6+} become larger.

Acknowledgments

This work was supported by the National Natural Science Foundation of China under Grant No. 11204376, No. 11274382 and No. 11274383.

References

- [1] Piancastelli M N 2013 *Eur. Phys. J. Special Topics* **222** 2035
- [2] Emma P *et al* 2010 *Nat. Photon.* **4** 641
- [3] Ishikawa T *et al* 2012 *Nat. Photon.* **6** 540
- [4] Bostedt C *et al* 2013 *J. Phys. B: At. Mol. Opt. Phys.* **46** 164003
- [5] Young L *et al* 2010 *Nature (London)* **466** 56
- [6] Berrah N *et al* 2010 *PNAS* **108** 16912
- [7] Fang L *et al* 2010 *Phys. Rev. Lett.* **105** 083005
- [8] Cryan J P *et al* 2010 *Phys. Rev. Lett.* **105** 083004
- [9] Salen P *et al* 2012 *Phys. Rev. Lett.* **108** 153003
- [10] Tamasaku K *et al* 2013 *Phys. Rev. Lett.* **111** 043001
- [11] Frasiniski L J *et al* 2013 *Phys. Rev. Lett.* **111** 073002
- [12] Santra R, Kryzhevoi N V and Cederbaum L S 2009 *Phys. Rev. Lett.* **103** 013002
- [13] Takahashi O and Ueda K 2014 *Chemical Physics* **440** 64
- [14] Ueda K and Takahashi O 2012 *J. Electron Spectroscopy Related Phenomena* **185** 301
- [15] Larsson M *et al* 2013 *J. Phys. B: At. Mol. Opt. Phys.* **46** 164030
- [16] Vinko S M *et al* 2012 *Nature (London)* **482** 59
- [17] Ciricosta O *et al* 2012 *Phys. Rev. Lett.* **109** 065002
- [18] Rackstraw D S *et al* 2014 *High Energy Density Phys.* **11** 59
- [19] Preston T R, Vinko S M, Ciricosta O, Chung H K, Lee R W and Wark J S 2013 *High Energy Density Phys.* **9** 258
- [20] Doumy G *et al* 2011 *Phys. Rev. Lett.* **106** 083002
- [21] Rohringer N *et al* 2012 *Nature (London)* **481** 488
- [22] Kanter E P *et al* 2011 *Phys. Rev. Lett.* **107** 233001
- [23] Ciricosta O, Chung H K, Lee R W and Wark J S 2011 *High Energy Density Phys.* **7** 111
- [24] Nikolopoulos G M and Lambropoulos P 2014 *J. Phys. B: At. Mol. Opt. Phys.* **47** 115001
- [25] Rohringer N and Santra R 2007 *Phys. Rev. A* **76** 033416
- [26] Abdallah Jr J, Colgan J and Rohringer N 2013 *J. Phys. B: At. Mol. Opt. Phys.* **46** 235004
- [27] Zeng J L and Yuan J M 2006 *Phys. Rev. E* **74** 025401(R)
- [28] Zeng J L and Yuan J M 2007 *Phys. Rev. E* **76** 026401
- [29] Zeng J L 2008 *J. Phys. B: At. Mol. Opt. Phys.* **41** 125702
- [30] Gao C, Zeng J L and Yuan J M 2011 *High Energy Density Phys.* **7** 54
- [31] Gao C, Zeng J L, Li Y Q, Jin F T and Yuan J M 2013 *High Energy Density Phys.* **9** 583
- [32] Gao C, Jin F T, Zeng J L and Yuan J M 2013 *New J. Phys.* **15** 015022
- [33] Xiang W J, Gao C, Fu Y S, Zeng J L and Yuan J M 2012 *Phys. Rev. A* **86** 061401(R)
- [34] Rose S J 2009 *High Energy Density Phys.* **5** 23
- [35] Gu M F 2008 *Can. J. Phys.* **86** 675
- [36] Zeng J L, Liu P F, Xiang W J and Yuan J M 2013 *Phys. Rev. A* **87** 033419

- [37] Zeng J L, Liu P F, Xiang W J and Yuan J M 2013 *J. Phys. B: At. Mol. Opt. Phys.* **46** 215002
- [38] Liu P F, Liu Y P, Zeng J L and Yuan J M 2014 *Eur. Phys. J. D* **68** 214
- [39] Gao C, Zeng J L and Yuan J M 2014 *Contrib. Plasma Phys.* doi: 10.1002/ctpp.201400061
- [40] Thomas T D, Shaw R W Jr 1974 *J. Electron Spectroscopy and Related Phenomena* **5** 1081
- [41] Bruch B, Schneider D, Chen M H, Chung K T and Davis B F 1992 *Phys. Rev. A* **45** 4476.
- [42] Ralchenko Yu, Kramida A E, Reader J and NIST ASD Team 2011 NIST Atomic Spectra Database (ver. 4.1.0), [Online]. Available: <http://physics.nist.gov/asd> [2012, May 1]. National Institute of Standards and Technology, Gaithersburg, MD
- [43] Gao C, Zeng J L and Yuan J M (submitted to *High Energy Density Phys.*)
- [44] Ackermann S *et al* 2013 *Phys. Rev. Lett.* **111** 114801
- [45] Li Y Q, Gao C, Dong W P, Zeng J L and Yuan J M 2015 arXiv: 1501.02660v1

Table 1. Single ionization potential (SIP) and double ionization potential (DIP) of SCH and DCH states for Ne-Ne⁹⁺ ions. The ground and single core-hole configurations are given to aid the understanding. Theoretical results are given except for those experimental values wherever available indicated after the ionization potentials.

Ion	Ground config.	SIP (eV)	SCH config.	DIP (eV)
Ne	1s ² 2s ² 2p ⁶	870.3[40]		
Ne ¹⁺	1s ² 2s ² 2p ⁵	892.6	1s2s ² 2p ⁶	986.0
Ne ²⁺	1s ² 2s ² 2p ⁴	923.1	1s2s ² 2p ⁵	1021.0
Ne ³⁺	1s ² 2s ² 2p ³	957.9	1s2s ² 2p ⁴	1061.2
Ne ⁴⁺	1s ² 2s ² 2p ²	1001.8[41]	1s2s ² 2p ³	1106.1
Ne ⁵⁺	1s ² 2s ² 2p	1048.5[41]	1s2s ² 2p ²	1152.3
Ne ⁶⁺	1s ² 2s ²	1099.1[41]	1s2s ² 2p	1202.3
Ne ⁷⁺	1s ² 2s	1143.2	1s2s ²	1253.6
Ne ⁸⁺	1s ²	1195.3[42]	1s2s	1311.6
Ne ⁹⁺	1s	1362.2		

Table 2. Resonance energy (RE) (eV) and weighted oscillator strength (gf) of 1s → 3p (1s²2s²2p³ → 1s2s²2p³3p, Nos. 1-9) and 1s → 2p (1s2s2p⁵ → 1s⁰2s2p⁶, Nos. 10-13) transitions for the production of SCH and DCH states of Ne³⁺ near 937 and 944 eV. Only those with gf larger than 0.02 near 937 eV and those larger than 0.1 near 944 eV are given for simplicity.

No.	Lower level	Upper level	RE	gf
1	[1s ² 2s ² 2p _{1/2} (2p _{3/2} ²) ₂] _{3/2}	[((1s2s ² 2p _{1/2}) ₁ (2p _{3/2} ²) ₂) ₁ 3p _{1/2}] _{1/2}	934.81	0.020
2	[1s ² 2s ² 2p _{1/2} (2p _{3/2} ²) ₂] _{3/2}	[((1s2s ² 2p _{1/2}) ₁ (2p _{3/2} ²) ₂) ₁ 3p _{3/2}] _{5/2}	934.82	0.047
3	[1s ² 2s ² 2p _{1/2} (2p _{3/2} ²) ₂] _{3/2}	[((1s2s ² 2p _{1/2}) ₁ (2p _{3/2} ²) ₂) ₁ 3p _{1/2}] _{3/2}	934.85	0.039
4	[1s ² 2s ² 2p _{1/2} (2p _{3/2} ²) ₂] _{5/2}	[((1s2s ² 2p _{1/2}) ₁ (2p _{3/2} ²) ₂) ₃ 3p _{3/2}] _{5/2}	930.88	0.107
5	[1s ² 2s ² 2p _{1/2} (2p _{3/2} ²) ₂] _{5/2}	[((1s2s ² 2p _{1/2}) ₁ (2p _{3/2} ²) ₂) ₂ 3p _{3/2}] _{7/2}	933.13	0.055
6	[1s ² 2s ² 2p _{1/2} (2p _{3/2} ²) ₂] _{3/2}	[(1s2s ² (2p _{3/2} ³) _{3/2}) ₁ 3p _{3/2}] _{3/2}	930.95	0.067
7	[1s ² 2s ² 2p _{1/2} (2p _{3/2} ²) ₂] _{3/2}	[((1s2s ² 2p _{1/2}) ₁ (2p _{3/2} ²) ₂) ₂ 3p _{1/2}] _{5/2}	933.11	0.039
8	[1s ² 2s ² (2p _{3/2} ³) _{3/2}] _{3/2}	[((1s2s ² 2p _{1/2}) ₁ (2p _{3/2} ²) ₀) ₁ 3p _{3/2}] _{1/2}	930.92	0.027
9	[1s ² 2s ² (2p _{3/2} ³) _{3/2}] _{3/2}	[(1s2s ² (2p _{3/2} ³) _{3/2}) ₁ 3p _{3/2}] _{5/2}	932.75	0.031
10	[(1s2s) ₀ (2p _{3/2} ³) _{3/2}] _{3/2}	[1s ⁰ 2s2p ⁶] _{1/2}	937.58	0.088
11	[(1s2s) ₁ (2p _{3/2} ³) _{3/2}] _{1/2}	[1s ⁰ 2s2p ⁶] _{1/2}	937.52	0.041
12	[(1s2s) ₁ 2p _{1/2}] _{3/2}	[1s ⁰ 2s2p ⁶] _{1/2}	944.98	0.506
13	[(1s2s) ₀ 2p _{1/2}] _{1/2}	[1s ⁰ 2s2p ⁶] _{1/2}	944.92	0.255

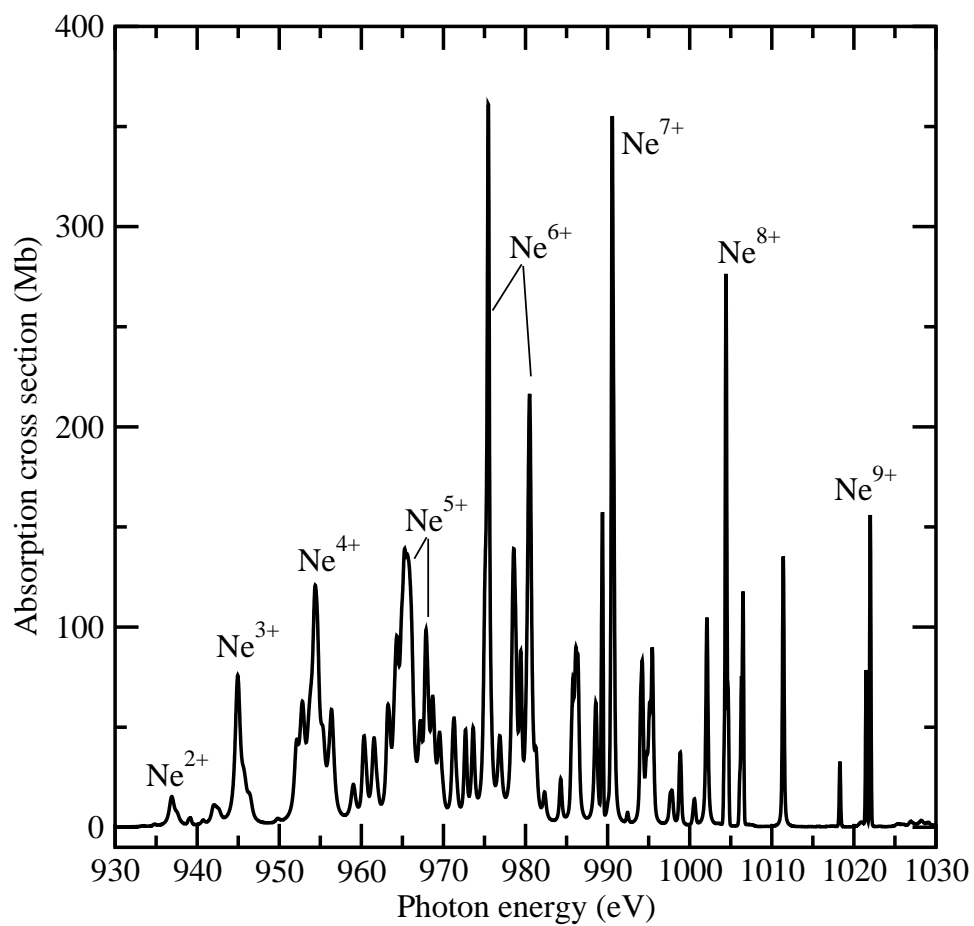


Figure 1. Absorption cross section (in Mb= 1.0×10^{-18} cm²) of $1s \rightarrow 2p$ resonance transitions from the SCH states $1s2s^m2p^n$ ($m + n = 8 - 1$) of neon charge states from Ne²⁺ to Ne⁸⁺. Note that Ne⁹⁺ has only one electron with the ground state of $1s$.

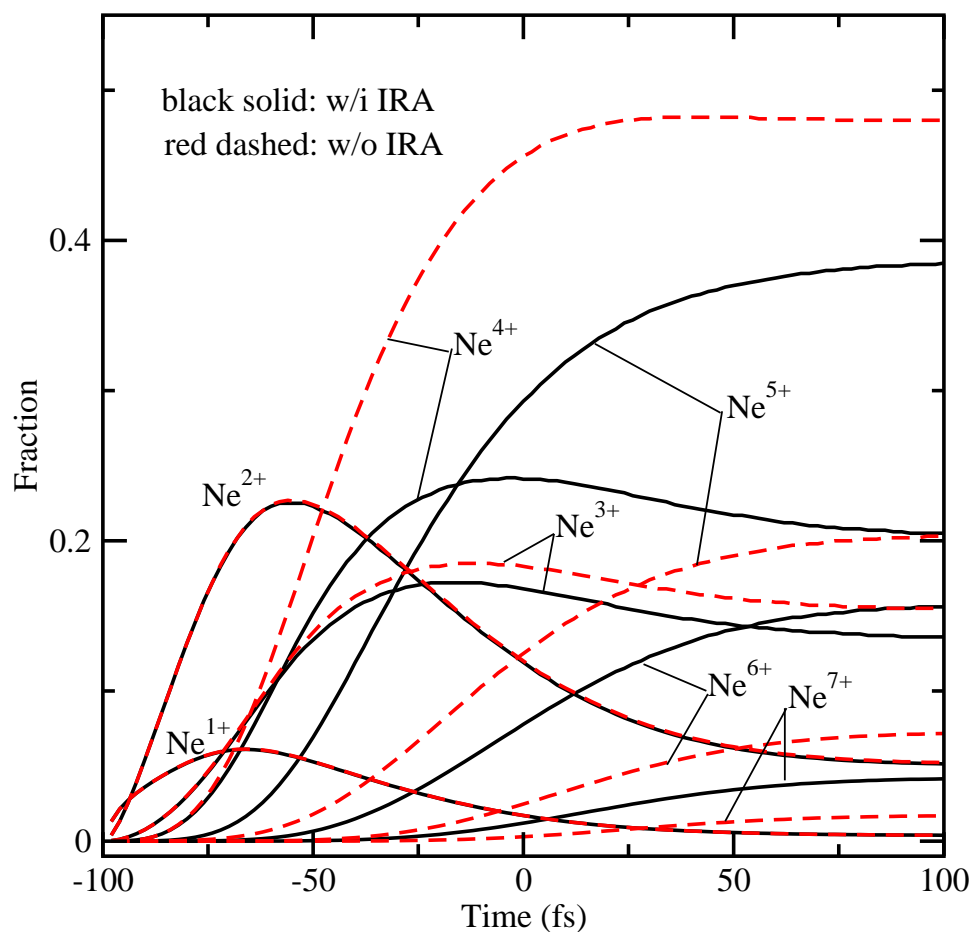


Figure 2. (Color online) Fraction evolution of neon charge states interacting with an x-ray pulse of peak intensity $I_0=2\times 10^{17}$ W/cm², duration $\tau=50$ fs with a central photon energy of 944 eV. The black solid and red dashed lines represent the results with and without IRA effects, respectively.

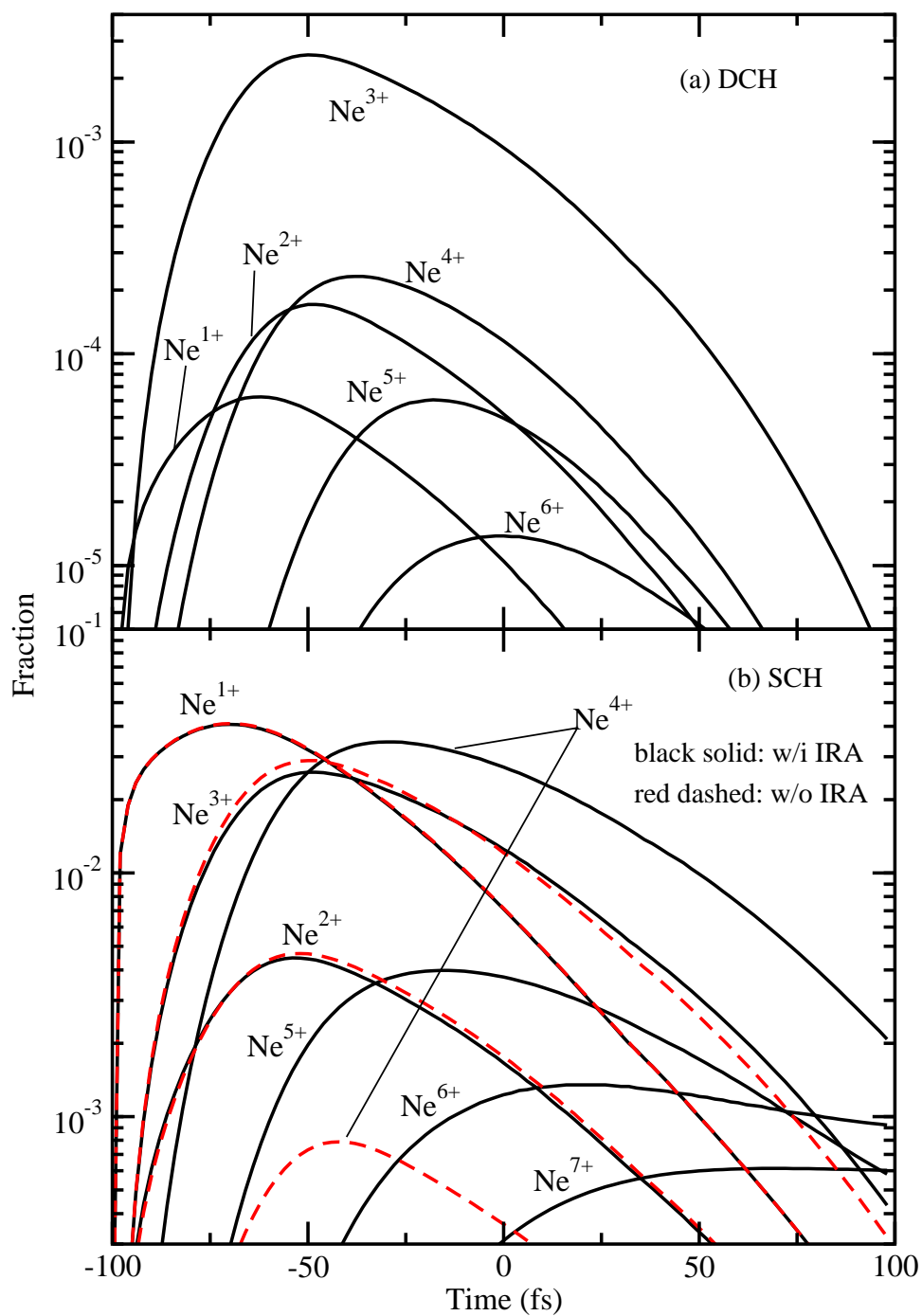


Figure 3. (Color online) Fraction evolution of (a) DCH and (b) SCH states of different neon charge states. The parameters of x-ray pulses are the same as in Fig.2. The black solid and red dashed lines represent the results with and without IRA effects, respectively. In panel (a), the populations of DCH states without IRA effects are too small to show. In panel (b), the populations of SCH states of Ne^{5+} - Ne^{7+} without IRA effects are not shown for the same reason.

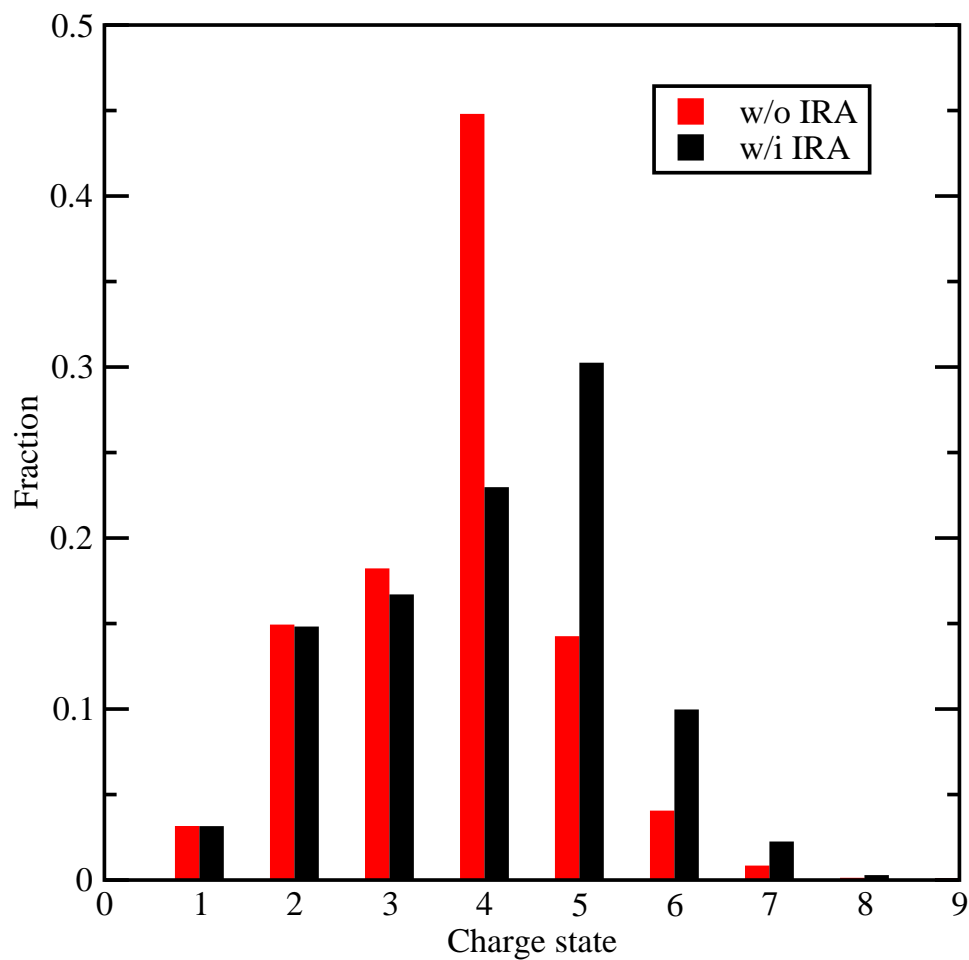


Figure 4. (Color online) Charge state distribution of neon after spatial and temporal averaging. The black and red bars represent the results with and without IRA effects, respectively. The parameters of the laser pulse are the same as in Fig. 2.

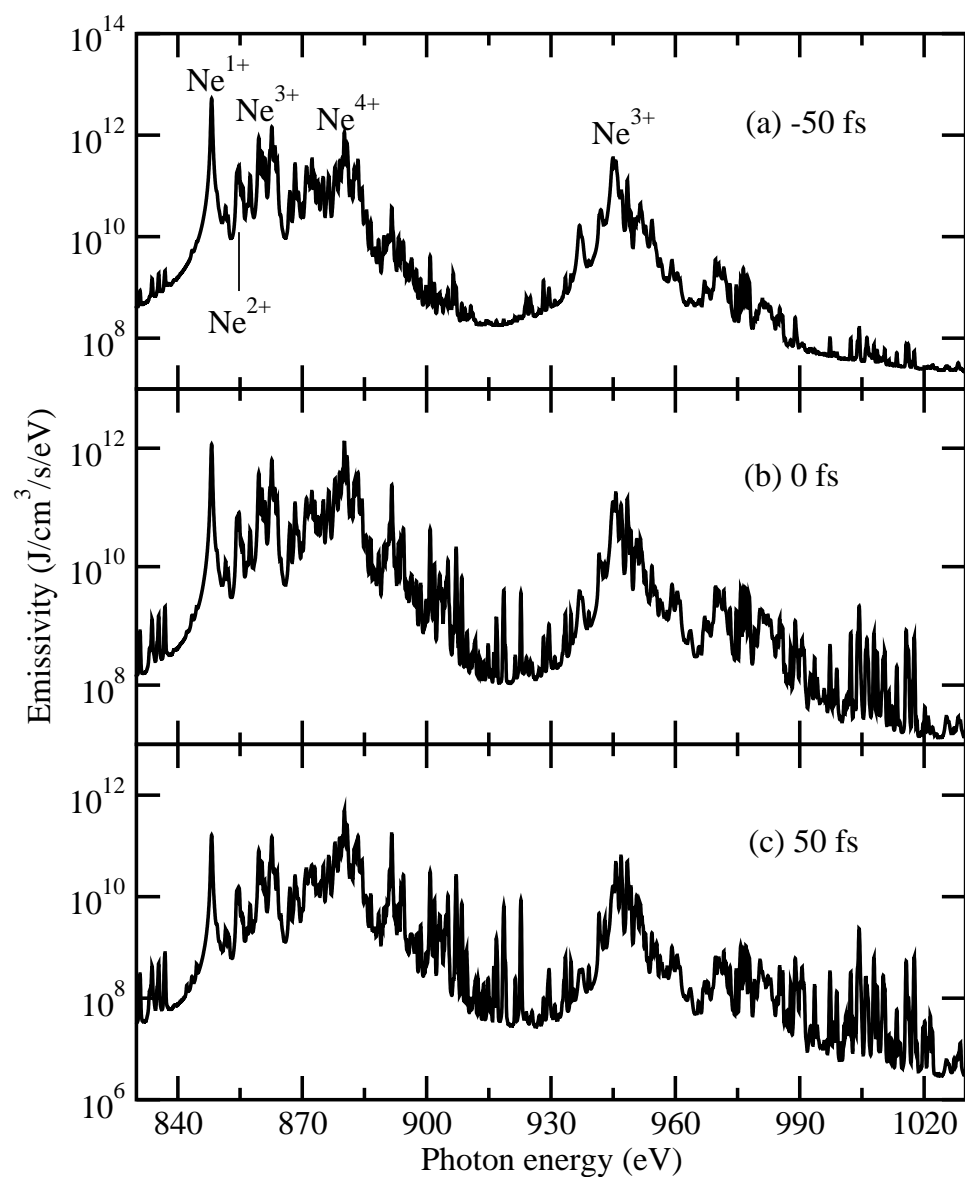


Figure 5. Emission spectra of SCH and DCH states of neon at time of (a) -50 , (b) 0 and (c) 50 fs in the photon energy range of 830 - 1030 eV. The parameters of the laser pulse are the same as in Fig. 2. The structures at lower photon energy range (<930 eV) are due to the SCH states and those at higher photon energy range (>930 eV) are dominantly due to the DCH states.

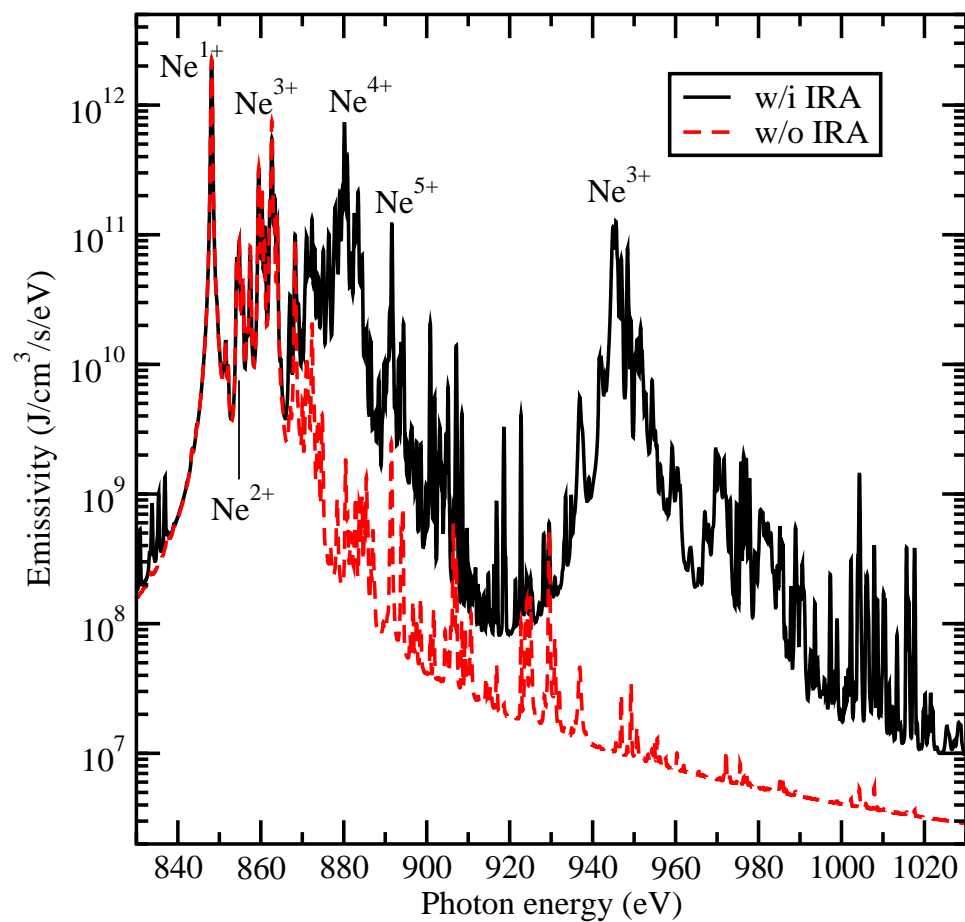


Figure 6. (Color online) Comparison between the emission spectra of neon with (black solid line) and without (red dashed line) IRA effects being considered after spatial and temporally averaging.

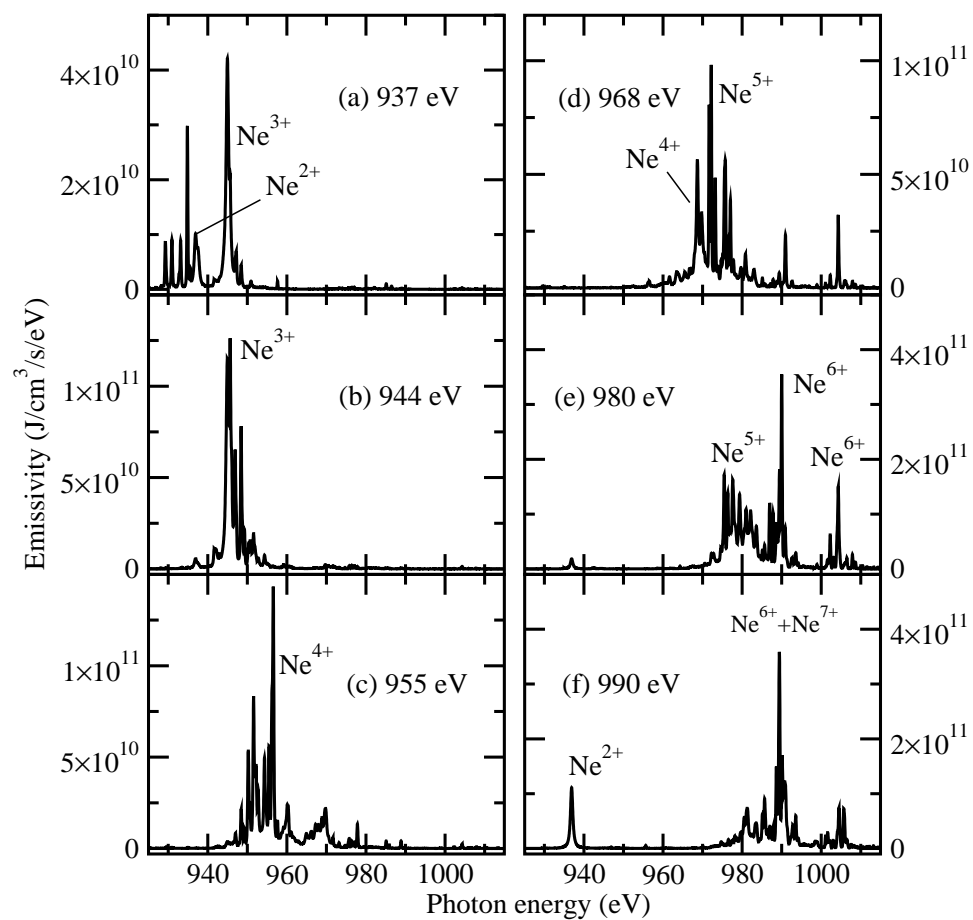


Figure 7. DCH emission spectra of neon interacting with x-ray pulses of peak intensity of 2×10^{17} W/cm², duration of 50 fs with photon energies of (a) 937 eV, (b) 944 eV, (c) 955 eV, (d) 968 eV, (e) 980 eV and (f) 990 eV, respectively.

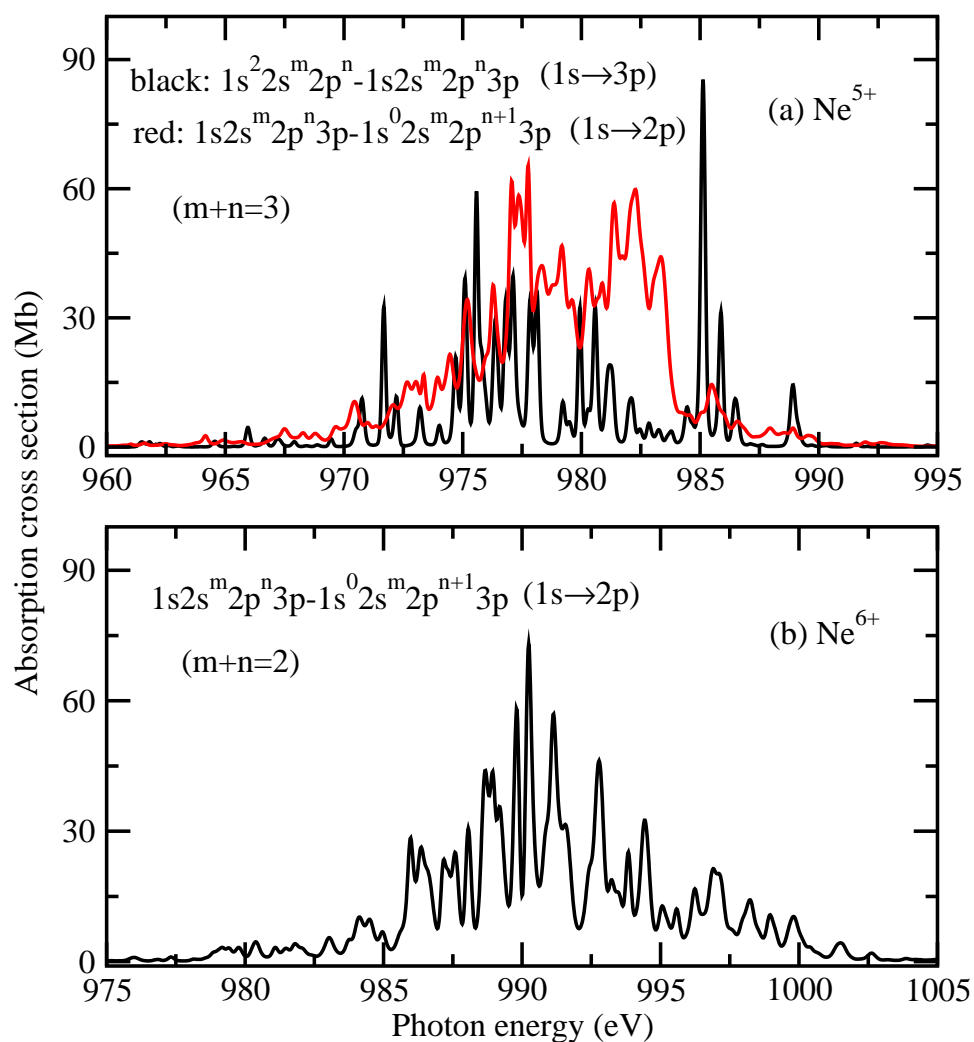


Figure 8. (Color online) Absorption cross section of (a) Ne^{5+} resonances of $1s^2 2s^m 2p^n \rightarrow 1s 2s^m 2p^n 3p$ and $1s 2s^m 2p^n 3p \rightarrow 1s^0 2s^m 2p^{n+1} 3p$ ($m+n=3$), and (b) Ne^{6+} from $1s 2s^m 2p^n 3p \rightarrow 1s^0 2s^m 2p^{n+1} 3p$ ($m+n=2$).

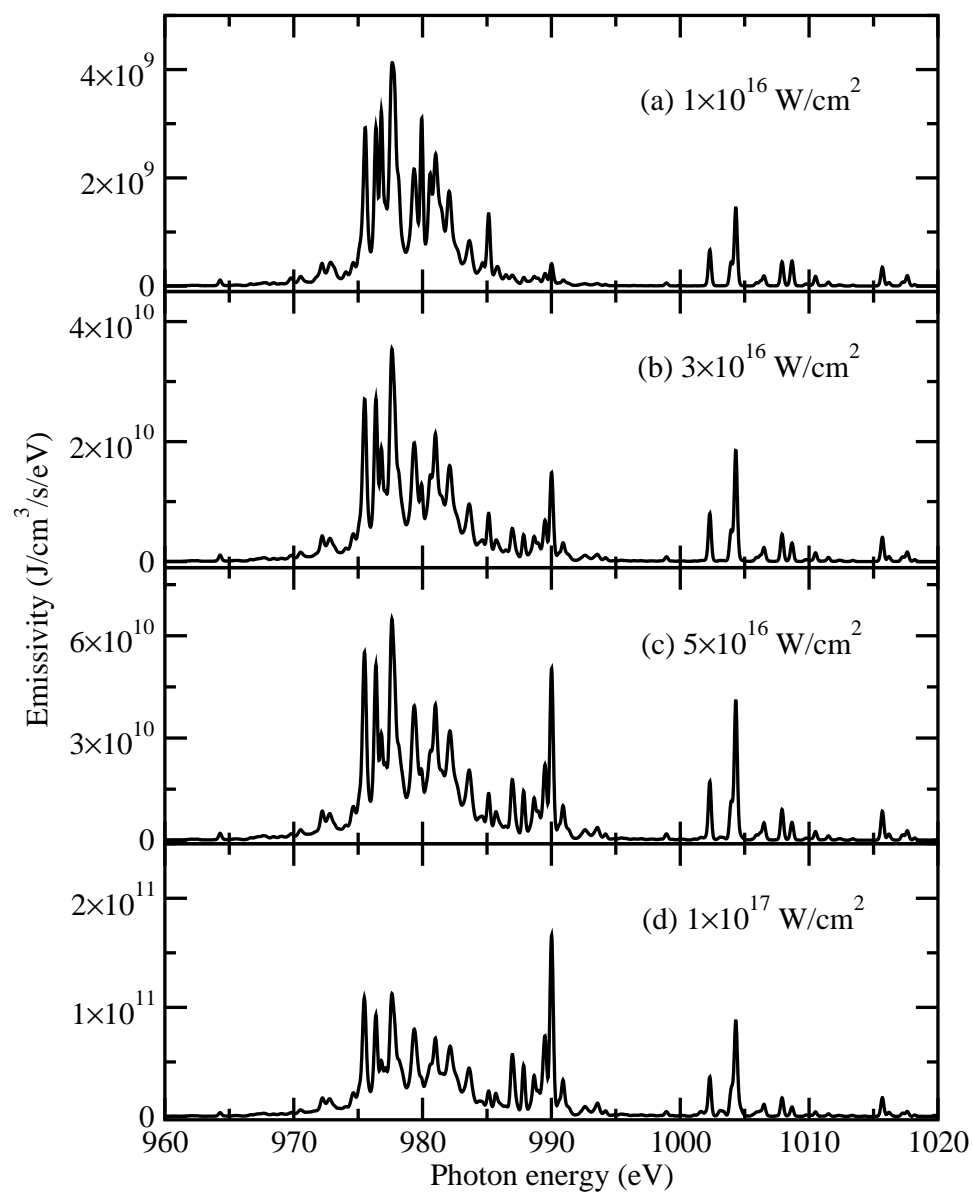


Figure 9. DCH emission spectra of neon interacting with x-ray pulses with photon energy of 980 eV, duration of 50 fs, and intensity of (a) 1×10^{16} , (b) 3×10^{16} , (c) 5×10^{16} and (d) 1×10^{17} W/cm², respectively.

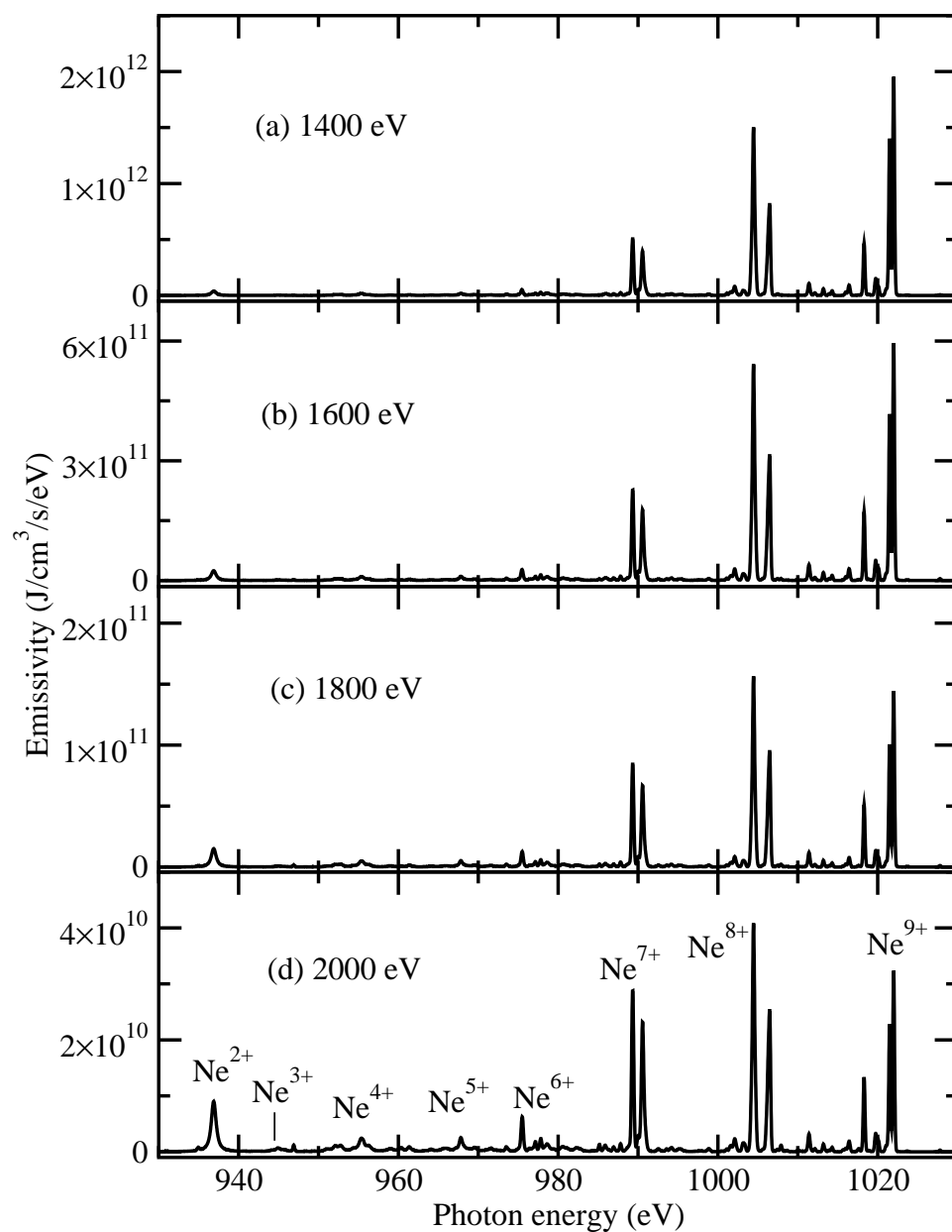


Figure 10. DCH emission spectra of neon interacting with x-ray pulses with photon energy of (a) 1400, (b) 1600, (c) 1800, and (d) 2000 eV. The parameters of the laser pulse are the same as in Fig. 2.